Pulsed-Bed Column Adsorption for Triclosan Removal Using Macadamia Nut Shell Activated Carbon

Jareeya Yimrattanabovorn [1*] , Mananya Phalaiphai [1], Siriwan Nawong [2]

[1] *School of Environmental Engineering, Suranaree University of Technology, Nakhon Ratchasima, 30000, Thailand.*

[2] *Synchrotron Research and Applications Division, Synchrotron Light Research Institute (Public Organization), Nakhon Ratchasima, 30000, Thailand.*

Abstract

Triclosan (TCS), a common antibacterial agent found in numerous personal care products, has been detected in wastewater and surface water and is now of significant environmental concern due to its health impacts. To mitigate this issue, various treatment methods have been explored. This study investigated the efficacy of Macadamia nut shell activated carbon (MAC) as an economical adsorbent for triclosan removal. A pulsed-bed column adsorption technique was applied to enhance adsorption capacity and prolong the operational lifespan of the column. Batch experiments were conducted to explore various parameters and adsorption capacity. Column experiments were carried out to investigate breakthrough curves and various associated parameters. In batch experiments, MAC exhibited a high TCS adsorption capacity of 119.05 mg/g, and optimal adsorption conditions were determined. Adsorption kinetics followed the pseudo-second-order model, and equilibrium data were well-fitted by both the Langmuir and Freundlich isotherm models. A pulsed-bed column adsorption showed superior performance compared to a fixed-bed column under specific conditions (flow rate: 10 mL/min, TCS initial concentration: 60 mg/L, bed column height: 10 cm) and removal bed height of only 6 cm, successfully enhancing TCS adsorption capacity to 53.40 mg/g and extending the operational lifespan of the column to 5,280 minutes. Adapting pulsed-bed columns for TCS removal from wastewater in the personal care product industry led to the extension of column life with increased adsorption capacity and minimized the use of adsorbents as a practical and environmentally friendly method.

Keywords: Macadamia Nut Shell Waste; Low-Cost Adsorbent; Triclosan; Pulsed-Bed Column; Fixed-Bed Column; Lifespan of Column.

1. Introduction

Triclosan (TCS), chemically identified as 5-chloro-2-(2,4-dichlorophenoxy) phenol, is a widely used antibacterial agent present in numerous products, especially personal care items. Its increasing presence in wastewater and water resources is now of significant environmental concern [1, 2], particularly heightened by the focus of the COVID-19 pandemic on sanitation and personal hygiene [2, 3]. Research has highlighted the adverse effects of TCS exposure on humans, aquatic life, and microbial communities, attributed to its ability to accumulate within their cells [4–7]. Studies conducted by Dar et al. (2022) [4] have elucidated pathways leading to the formation of harmful by-products resulting from the interaction of triclosan with photodegradation, chlorination, and oxidation processes. These reactions involve the insertion of chlorine atoms into para and ortho positions, yielding compounds such as 2,8-dichlorodibenzo-p-dioxin (DCDD), 2,4,6-trichlorophenol (2,4,6 TCP), and polychlorodibenzo-p-dioxins (PCDD) [8].

Numerous studies have investigated various techniques for eliminating triclosan (TCS). However, some of these methods' present challenges, such as bioaccumulation or the formation of toxic by-products. Photodegradation and

oxidation can generate harmful by-products [4-6, 8]. Adsorption has emerged as a promising alternative for TCS removal, offering the advantage of producing non-toxic by-products [9, 10]. Activated carbon is a widely favored adsorbent due to its exceptional capacity, but it generates higher production costs. To address this challenge, researchers have developed various natural adsorbents, including Macadamia nut shell activated carbon (MAC) as a cost-effective adsorbent derived from agricultural waste, which demonstrates high surface area and cost-effectiveness [11]. Previous studies have shown MAC to be effective for phenol adsorption [12, 13].

Adsorption techniques include both batch and continuous fixed-bed methods, with the latter being preferred in industrial applications because of its operational simplicity and scalability [14, 15]. Column adsorption, such as fixed-bed columns, is used for industrial wastewater treatment because it is simple to operate with continuous flow and fast adsorption and can be achieved with a high loading of pollutants due to a given large amount of fresh adsorbent in the column [16]. However, fixed-bed columns have limitations such as potential obstructions and decreased efficiency over time, requiring sorbent material replacement. A clogging problem on the column decreases column life extension, and high dosages of adsorbent waste limit the use of this system, resulting in lower adsorption capacity compared to batch adsorption and leading to underutilization and waste [16, 17].

This study introduced a groundbreaking alternative: the pulsed-bed column adsorption system with enhanced adsorption capacity. The pulsed-bed system selectively releases the less efficient column bed height as it becomes partially depleted and introduces regenerated fresh adsorbent, allowing more comprehensive utilization of adsorbent and reducing consumption. This innovative approach extends the operational lifespan of adsorbents in column adsorption processes [17, 18].

The objectives of this investigation were to assess the practicality of using MAC as a cost-effective adsorbent derived from agricultural waste for triclosan removal through batch and column adsorption studies, with a focus on an alternative pulsed-bed column adsorption system. Batch experiments explored various parameters to determine the optimal conditions for fixed-bed columns, including initial TCS concentration, contact time, initial pH, and agitation speed, along with adsorption isotherms, thermodynamics, and kinetics studies. Column experiments involved breakthrough curves and associated parameters under different initial TCS concentrations, flow rates, and bed heights. Fixed-bed column studies provide crucial insights for adapting parameters to pulsed-bed column applications for TCS removal from wastewater in the personal care product industry, leading to an extension of column life, increased adsorption capacity, and minimized use of adsorbent as a practical and environmentally friendly method for TCS removal.

2. Material and Methods

A study framework was designed to investigate the use of MAC as an adsorbent for TCS removal through batch and column adsorption experiments, as illustrated in Figure 1. The analysis included evaluating adsorbent characteristics, examining adsorption data, predicting column behavior, and conducting XTM analysis for data interpretation.
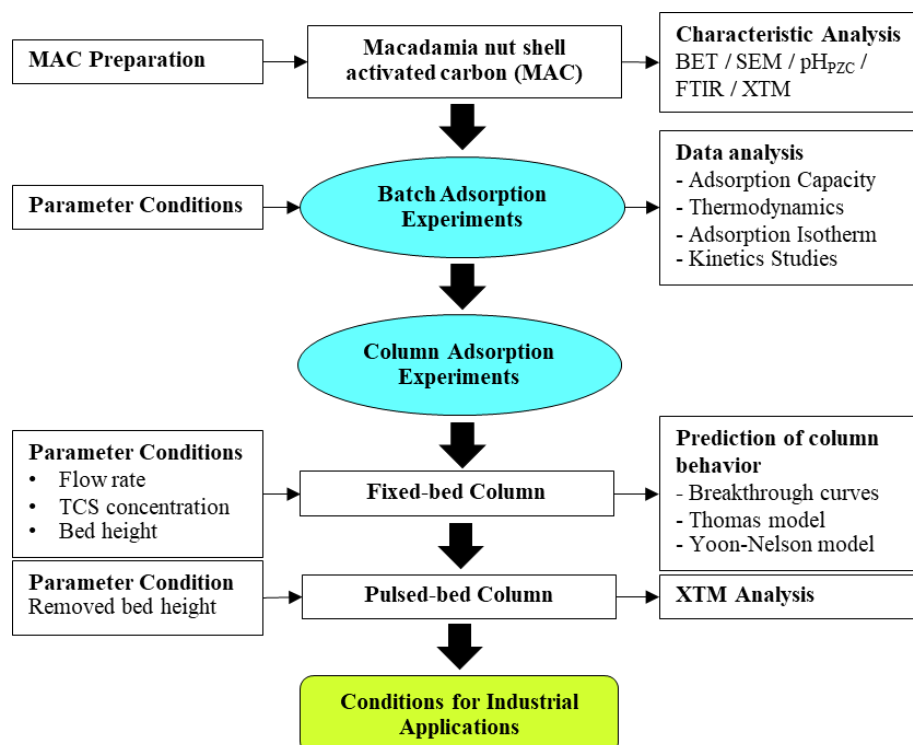

Figure 1. Schematic Flowchart of the Study Framework

2.1. Preparation of Macadamia Nut Shell Activated Carbon (MAC) as an Adsorbent Material

The macadamia nut shell charcoal utilized in this study was sourced from Khaokho district in Phetchabun Province, Thailand. The process of preparing MAC followed the methodology in our previous research. Carbonization was conducted at 950°C using CO_2 gas at a flow rate of 200 mL/min with an activation time of 240 minutes. The MAC samples were characterized using the Brunauer-Emmett-Teller (BET) method, employing a Belsorp Mini II instrument from Japan. The functional groups of MAC before and after adsorption were identified through synchrotron IR analysis at BL4.1 Infrared Spectroscopy and Imaging, conducted at the Synchrotron Light Research Institute (SLRI). Infrared spectra were acquired using an infrared microscope (Hyperion 2000, VERTEX 70, Bruker. Optics, Ettlingen, Germany) with a 36x IR objective, covering a wave number range of 4000 to 800 cm^{-1}. Spectral analysis was performed using OPUS 7.2 software (Bruker Optics Ltd., Ettlingen, Germany).

2.2. Material Preparation of TCS as an Adsorbate and Analytical Methods

TCS powder with a purity exceeding 97% was acquired from Thermo Fisher Scientific Inc. (Waltham, USA). A stock solution at a concentration of 200 mg/L was prepared by dissolving the powder in 0.1 M NaOH in deionized water. This solution was carefully stored in the dark at 4°C to shield it from sunlight. The concentration of TCS was quantified using the diazotization method [19, 20]. The concentration of TCS was measured at 445 nm by a UV/Visible spectrophotometer (JENWAY 7315, UK).

2.3. Batch Adsorption Experiments

The batch adsorption experiments utilized 250 mL conical flasks, each containing 200 mL of TCS solution. The flasks were placed within a thermostat shaker. Detailed experimental conditions are provided in Table 1. The primary goal was to investigate how initial TCS concentration, contact time, initial pH, and agitation speed influenced TCS adsorption.

Table 1. Overview of parameters used in batch adsorption experiments

Experiments	Parameters				
	Contact time (min)	Initial concentration (mg/L)	Agitation speed (rpm)	Temperature (°C)	Initial pH
Effect of contact time	60-1,080	20	150	30	10.5±0.2
Effect of initial concentration	780	2-20	150	30	10.5±0.2
Effect of agitation speed	780	20	50-200	30	10.5±0.2
Effect of temperature	780	20	150	25-45	10.5±0.2
Effect of initial pH	780	20	150	30	2-12

C_0 as the initial concentration (mg/L) and C_e as the remaining concentration (mg/L) of TCS were measured to calculate the amount of TCS adsorbed onto MAC. The equilibrium adsorption capacity was denoted as q_e (mg/g), using Equation 1, where V signifies the volume of the TCS solution (mL), and m denotes the weight of MAC (g).

$$q_e = \frac{(C_0 - C_e)V}{m} \tag{1}$$

During these batch experiments, the key thermodynamic parameters including ΔG° as Gibbs free energy (kJ/mol), ΔS° as entropy change (kJ/mol-K), and ΔH° as enthalpy change (kJ/mol) were determined temperatures ranging from 298 to 318 K (Equations 2 and 3). In these equations, K represents the equilibrium constant of the isotherm fits, R is the gas constant (8.314 J/mol/K), and T is the absolute temperature (K). The values of ΔH° were derived from the slope of ΔH°/R, while ΔS° was determined from the intercept of $\Delta H^0/R$ in the linear plot of ln K versus 1/T.

$$(\Delta G°) = -RT \ln K \tag{2}$$

$$\ln K = \frac{\Delta S°}{R} - \frac{\Delta H°}{RT} \tag{3}$$

2.4. Adsorption Isotherm and Kinetics

Various TCS concentrations ranging from 5 to 60 mg/L were tested using 200 mL of TCS solution and MAC weight of 0.1 g. The initial pH of the solution was maintained at 2 and 10.5±0.2, and experiments were carried out at ambient temperature (approximately 30°C) and 45°C. The adsorption capacity was determined using the linear forms of the Langmuir and Freundlich isotherms. The Langmuir isotherm is expressed by the linearized Equation 4:

$$\frac{C_e}{q_e} = \frac{C_e}{q_m} + \frac{1}{K_L q_m} \tag{4}$$

In this context, q_m corresponds to the maximum TCS sorbed (mg/g), and K_L stands for the Langmuir constant (L/mg). In the Freundlich isotherm, captured by the linearized Equation 5, K_F is the Freundlich constant $(mg/g)(L/mg)^{1/n}$, and n signifies the Freundlich exponent.

$$\log q_e = \log K_F + \frac{1}{n} \log C_e \tag{5}$$

Kinetics were explored by applying pseudo-first-order and pseudo-second-order models, expressed in their linearized forms in Equations 6 and 7, respectively.

$$\ln(q_e - q_t) = \ln q_e - k_1 t \tag{6}$$

$$\frac{t}{q_t} = \left(\frac{1}{k_2 q_e}\right)^2 + \frac{t}{q_e} \tag{7}$$

In these equations, q_t denotes the quantities of TCS (mg/g) at any given time, t (minutes). The parameter k_1 represents the pseudo-first-order rate constant (min^{-1}), which can be derived from the plot of $\ln(q_e - q_t)$ against t. Similarly, k_2 is the pseudo-second-order rate constant (g/mg-min), determined from the plot of t against t/q_t.

2.5. Fixed-bed Column Adsorption Experiments

Fixed-bed column adsorption experiments were conducted using an acrylic tube with a 2 cm internal diameter and a height of 10 cm, as illustrated in Figure 2. These experiments employed a continuous up-flow operation using a peristatic pump and the initial pH of the TCS solution was controlled at 10.5±0.2 by adjusting with either 0.1M NaOH or 0.1M HCl. The entire experiment took place under ambient temperature conditions.
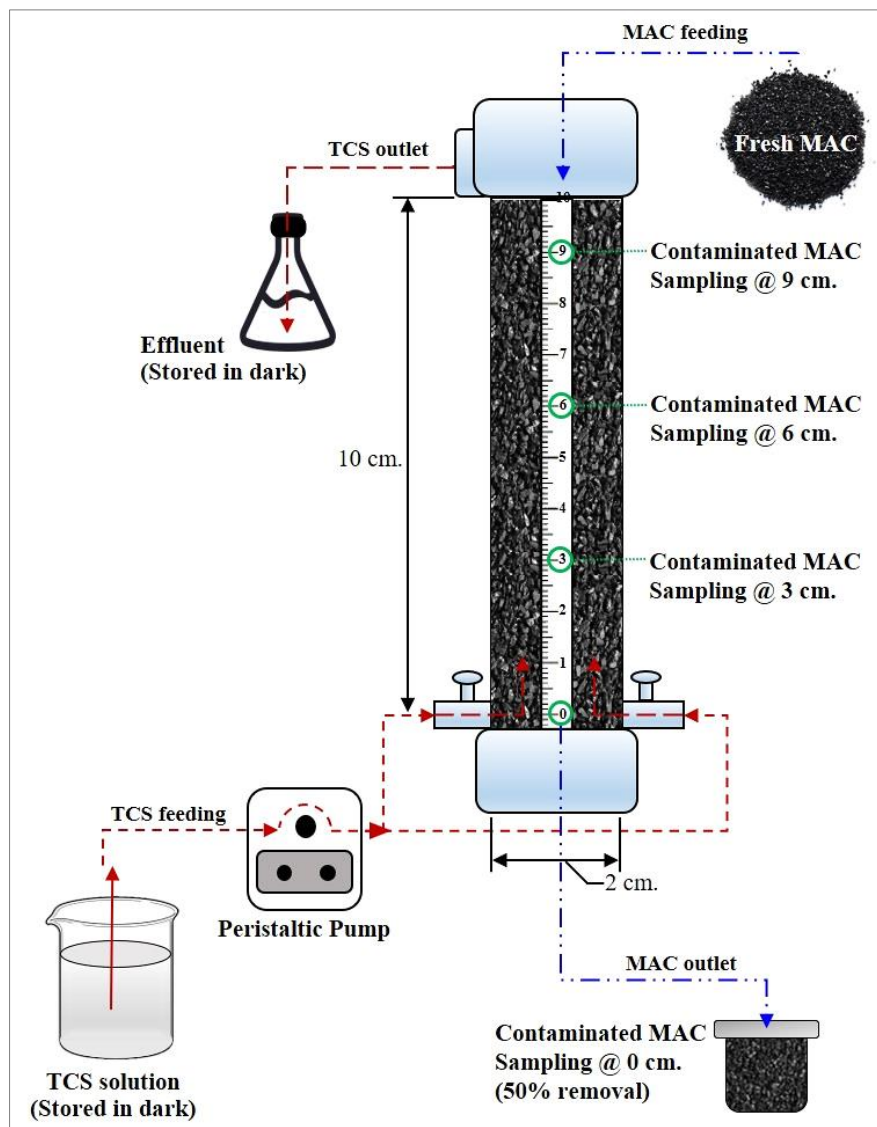

Figure 2. Schematic flowchart of column adsorption experiments

The fixed-bed column experiment encompassed diverse conditions including varying flow rates (6, 8, and 10 mL/min), initial TCS concentrations (20, 40, and 60 mg/L), and different fixed-bed heights (6, 8, and 10 cm). The objective of this study was to investigate the continuous adsorption process at two crucial points: achieving 95% removal ($C_e/C_0 = 0.05$) and 5% removal ($C_e/C_0 = 0.95$) on the breakthrough curve. Supernatant analysis was conducted to determine the residual concentration of TCS. Breakthrough curves were plotted, illustrating C_t/C_0 against time. Various parameters such as t_b breakthrough time (minutes), t_s saturation time (minutes), V_{eff} effluent volume (L), q_b adsorption at breakthrough (mg/g), and q_s adsorption at saturation (mg/g) were computed.

The analysis of breakthrough curves involved the application of the Thomas and Yoon-Nelson models. These models provide valuable insights into the relationship between the rate of adsorption and the breakthrough on the adsorbent. This mathematical relationship is described by the linearized Equations 8 and 9 for the Thomas and Yoon-Nelson models, respectively.

$$\ln\left(\frac{C_t}{C_0} - 1\right) = \frac{K_{TH}q_{TH}m}{Q} - K_{TH}C_0 t \tag{8}$$

$$\ln\left(\frac{C_t}{C_0} - C_t\right) = K_{YN}t - \tau K_{YN} \tag{9}$$

In these equations, C_t represents the amounts of TCS (mg/L) at any time, m is the MAC weight used in the column (g), Q is the feed flow rate (mL/min), and K_{TH} and q_{TH} represent the Thomas rate constant (mL/mg-min) and the equilibrium TCS uptake (mg/g). Following Equation 8, the Thomas constant values of K_{TH} and q_{TH} can be obtained from the slope and intercept of the linear plot of ln (C_t/C_0 - 1) versus t at different flow rates, initial concentrations, and bed heights. On the other hand, following Equation 9, K_{YN} represents the Yoon-Nelson rate constant (min⁻¹), t is the time required for contaminant breakthrough (minutes), and τ is the time required for 50% adsorbate breakthrough (minutes). The values of K_{YN} and t can be obtained from the linear plot of ln (C_t/C_0 - C_t) versus t. The data resulted in a slope of K_{YN} and an intercept of τK_{YN}.

2.6. Pulsed-Bed Column Adsorption Experiments

A flowchart illustrating the pulsed-bed column adsorption experiments is presented in Figure 2. The experiment was conducted based on the conditions determined from the fixed-bed column study. Various removed pulsed-bed heights ranging from 2, 4, and 6 cm were assessed for adsorption capacity and operational lifespan of the column. The column bed was replaced upon reaching 50% removal ($C_e/C_0 = 0.50$), and fresh MAC was introduced at the top corresponding to the amount of MAC removed. The experiment consisted of a total of 4 cycles, and parameters of the breakthrough curve were subsequently calculated.

2.7. Clogging Pattern Analysis

Fresh and contaminated MAC samples were collected after the completion of the fourth feeding cycle in the pulsed-bed experiment, at depths of 0, 3, 6, and 9 cm from the bottom of the column. These collected samples underwent analysis to determine total porosity, open porosity, and closed porosity using X-ray Tomographic Microscopy (XTM) with a synchrotron X-ray source known as BL1.2W, which integrates X-ray imaging and XTM capabilities. The collected X-ray radiographs were analyzed using Octopus Reconstruction software (TESCAN, Gent, Belgium), resulting in the generation of reconstruction images. The analysis covered a volume with a total size of 0.219 mm³. These reconstruction images were processed using Drishti software to create a three-dimensional tomographic reconstruction. The accuracy of the findings was confirmed through collaboration with the Synchrotron Light Research Institute in Thailand.

3. Results and Discussions

3.1. Characterization of the MAC

Analysis of freshly acquired MAC samples, as revealed by BET analysis, indicated a BET surface area of 985.40 m²/g, a total pore volume of 0.4269 cm³/g, a pore diameter of 2.15 nm, and an impressive 93% of the volume comprised of micropores.

3.2. Batch Adsorption Experiments

3.2.1. Effect of Contact Time, Initial Concentration, Agitation Speed and Temperature

As depicted in Figures 3-a and 3-b, a significant rise in adsorption capacity was evident with an increase in both TCS concentration and contact time. This swift adsorption was attributed to the abundance of active sites on the MAC surface. Higher concentrations contributed to an intensified driving force, thereby facilitating the rapid diffusion of TCS molecules into the pores [13, 21]. The adsorption capacity continued to increase until reaching saturation at 780 minutes, demonstrating a final adsorption capacity of 27.80 mg/g.
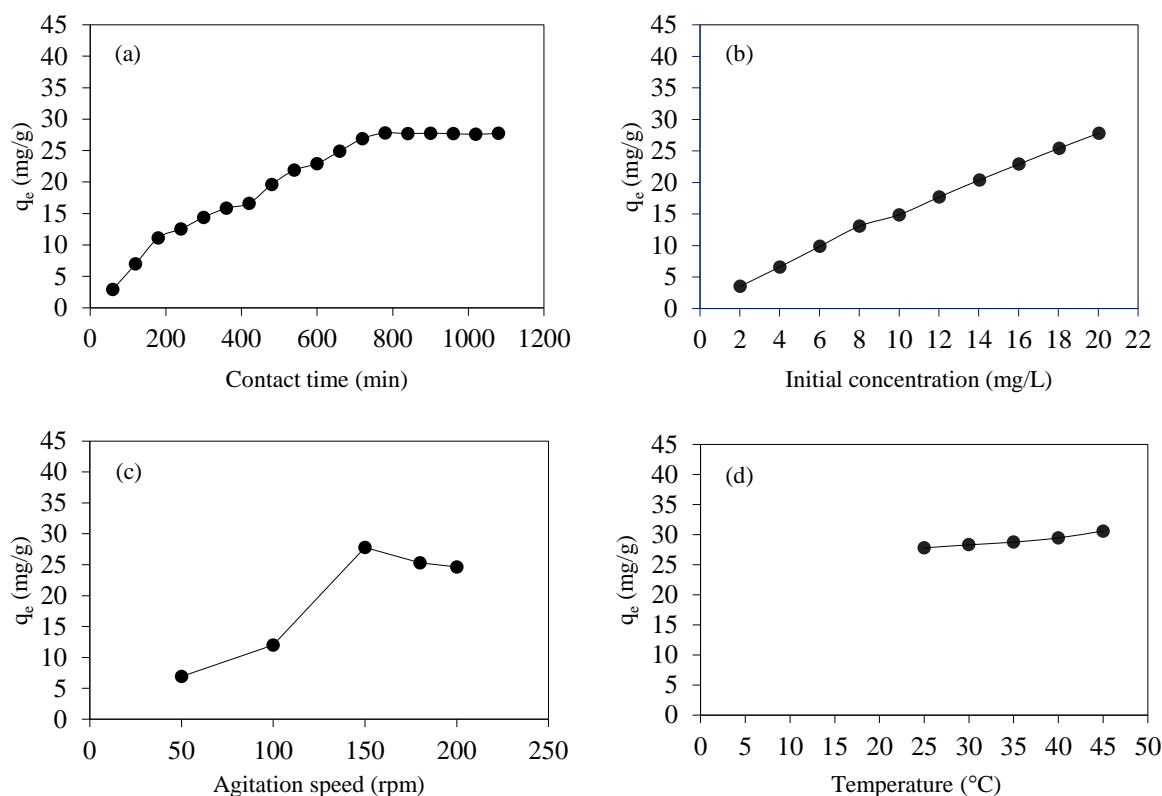
Figure 3. Effect of (a) contact time, (b) initial concentration, (c) agitation speed, and (d) temperature on TCS adsorption

The adsorption capacity showed a consistent increase as the agitation speed escalated, eventually reaching equilibrium at 150 rpm (Figure 3-c). However, beyond this point, the adsorption capacity declined with a further increase in agitation speed to 200 rpm. This decline was primarily attributed to a reduction in the boundary layer thickness surrounding the adsorbent, as discussed by Karthika and Vasuki (2021) [22]. An elevation in temperature correlated with improved adsorption (Figure 3-d), suggesting an endothermic adsorption process. Higher temperatures enhanced the mobility of TCS, facilitating diffusion through the external boundary film and into the inner pores of MAC. Higher temperatures also resulted in a decrease in solution viscosity [23]. However, industrial application of the 45°C temperature range may involve heightened costs.

Therefore, the parameters selected for subsequent batch adsorption experiments included an initial TCS concentration of 20 mg/L, a contact time of 780 minutes, and an agitation speed of 150 rpm. These experiments were conducted at both ambient temperature and 45°C.

3.2.2. Effect of Initial pH

Results revealed that the adsorption capacity reached a peak under acidic conditions (pH 2–6) at both temperatures, ranging from 35.24 to 40.00 mg/g (Figure 4). Heightened adsorption in acidic environments was ascribed to hydrophobic interactions between the MAC surface and phenolic-TCS, along with pore filling, hydrogen bonding, and π-π bonding. TCS demonstrated the capacity to self-couple with the oligomer [24].
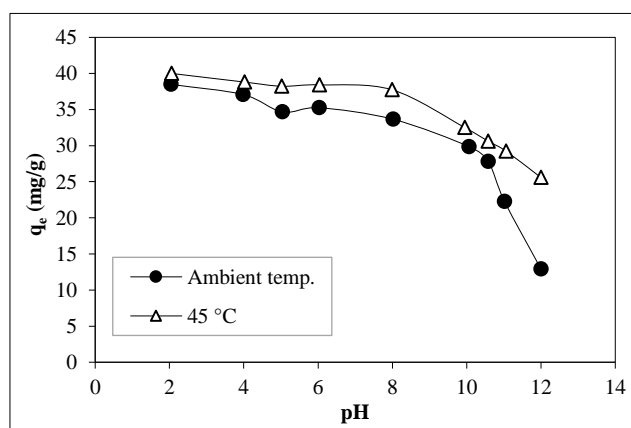
Figure 4. Impact of initial solution pH at ambient temperature and 45°C on TCS adsorption onto MAC

FTIR results of MAC after adsorption at pH 2-6 (Figure 5) displayed peaks in the hydroxyl and aliphatic hydrocarbon stretching vibration ranges of 3600-3100 and 3000-2850 cm^{-1}, respectively, likely associated with hydrogen bonding. Peaks of C=C observed in the range 1600-1450 cm^{-1} indicated the reaction between the TCS ring and the MAC surface (π-π reaction), leading to enhanced stability [25, 26]. These peaks were verified in MAC spectra after the adsorptive process, indicating the presence of TCS.
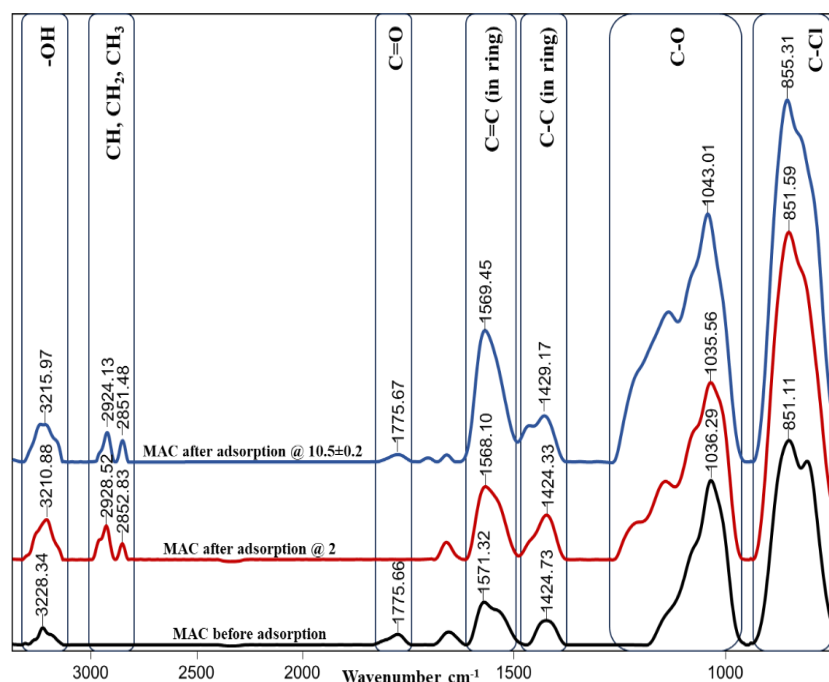

Figure 5. FTIR spectrum analysis of MAC before and after TCS adsorption at initial pH solutions of 2 and 10.5±0.2

A significant decrease in adsorption capacity was noticeable under alkaline conditions (pH 8–12), ranging from 37.75 to 12.91 mg/g. This reduction was attributed to the modulation of surface charges on the adsorbent, resulting in subsequent alterations in the adsorbate state [27]. The study identified the pH at which the MAC reached its point of zero charge (pH$_{PZC}$) as 7.9, indicating a negatively charged surface beyond this point [28, 29]. Under alkaline conditions, TCS undergoes deprotonation, transforming into the anionic form, phenolate-TCS [26, 30, 31].

Thus, in alkaline environments, the MAC surface acquires a negative charge, while TCS exists in a deprotonated anionic state. This results in enhanced electrostatic repulsion between the triclosan anions and the negatively charged MAC surface, as indicated by the adsorbents' point of zero charge. This phenomenon elucidates the decreased adsorption capacity observed at these pH values. In such conditions, electrostatic repulsion becomes the primary interaction, resulting in a decline in adsorption capacity with increasing pH. This finding was supported by Vidovix et al. (2022) [26].

To optimize cost efficiency and minimize energy consumption, it is crucial to avoid extensive pH adjustments, especially considering that the pH of wastewater in the personal care products industry is in the range of 9–11. Therefore, for practical application in fixed-bed column experiments within a factory setting, the chosen conditions involve an initial solution pH of 10.5±0.2, ambient temperature, TCS initial concentration of 20 mg/L, contact time of 780 minutes, and agitation speed of 150 rpm. These optimal conditions were selected to achieve a high TCS adsorption capacity in subsequent column adsorption experiments, as well as for potential industrial applications and to align with the characteristics of the wastewater.

3.3. Adsorption Isotherms

The experimental adsorption data were analyzed using the Langmuir and Freundlich isotherms, with the corresponding parameters presented in Table 2. Both isotherms exhibited strong correlation coefficients, with values ranging from 0.9245 to 0.9948 for Langmuir and 0.9582 to 0.9864 for Freundlich, indicating a good fit in both cases. Based on the Langmuir isotherm analysis, the maximum adsorption capacity was determined to be within the range of 90.09 to 119.05 mg/g. To validate the adsorption of TCS on the MAC surface, SEM micrograph images of MAC samples were examined before and after adsorption, as depicted in Figure 6. The micrograph illustrates that the surface pores of MAC after adsorption (Figure 6-b) were covered with pollutant molecules, contrasting with the clear pores observed on MAC before adsorption (Figure 6-a).

BET analysis revealed that MAC before adsorption had an impressive 93% of the volume comprised of micropores. Kaur et al. (2018) [32] reported TCS molecular dimensions of 1.42×0.69×0.75 nm. This discovery supported the feasibility of TCS accessing the MAC micropores. Based on the 3D visualization of MAC from the XTM analysis presented in Figure 7-b, the post-adsorption MAC displayed enhanced connectivity in the green area, representing air as the dispersive phase, and appeared narrower compared to the MAC before adsorption (Figure 7-a). This narrowing was attributed to the increased presence of TCS molecules diffused onto the MAC, thereby expanding the brown area, depicted as the matrix phase. As depicted in Figure 8, the integral areas of the FTIR spectrum indicated that the MAC after adsorption at pH 2 exhibited higher amounts of -OH, C-O, and C-Cl compared to both the MAC before adsorption and at pH 10.5±0.2 conditions. This provided strong evidence of a significant adsorption process. Therefore, both chemical and physical interactions, including H-bonding, π-π reactions, electrostatic forces, and surface diffusion, were deemed crucial in facilitating the adsorption process. These collective results supported the conclusion that TCS adsorbed on the MAC surface, as supported by previous studies [26, 33].

Table 2. Langmuir and Freundlich parameters for TCS adsorption on MAC

pH	Temp. (ºC)	$q_{e, exp}$ (mg/g)	Langmuir isotherm			Freundlich isotherm		
			q_m (mg/g)	K_L (L/mg)	R^2	n	K_F (mg/g)(L/mg)$^{1/n}$	R^2
2	30	98.79	102.04	0.29	0.9551	1.61	22.67	0.9713
2	45	109.30	119.05	1.00	0.9245	2.80	58.64	0.9582
10.5±0.2	30	75.36	90.09	0.07	0.9948	1.45	7.38	0.9864
10.5±0.2	45	91.65	98.04	0.13	0.9846	1.59	13.15	0.9848
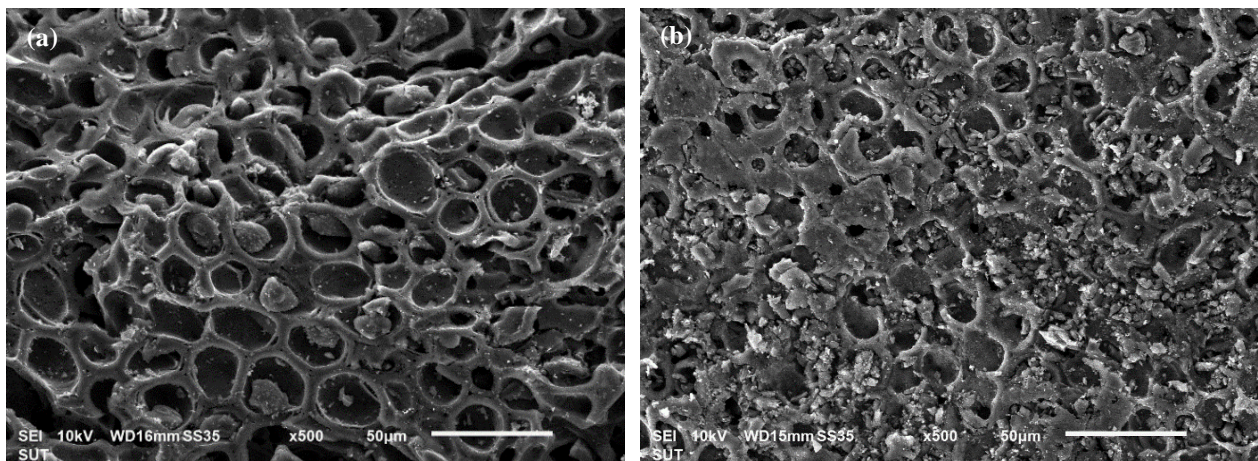
Figure 6. SEM analysis at 500x magnification (a) MAC before adsorption, and (b) MAC after adsorption
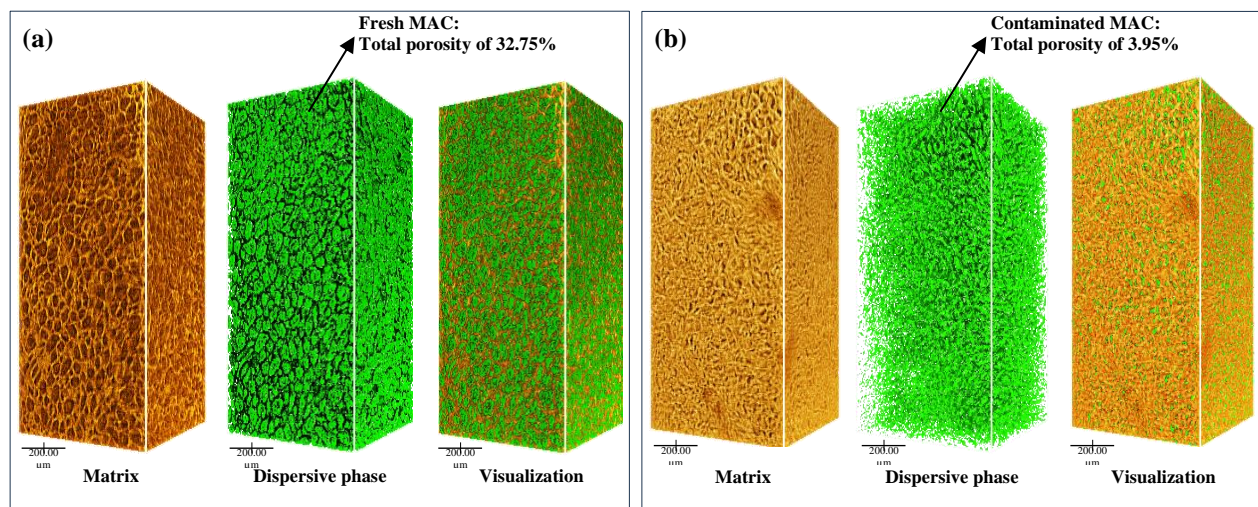
Figure 7. 3D visualization of MAC from XTM analysis (a) MAC before adsorption, and (b) MAC after adsorption
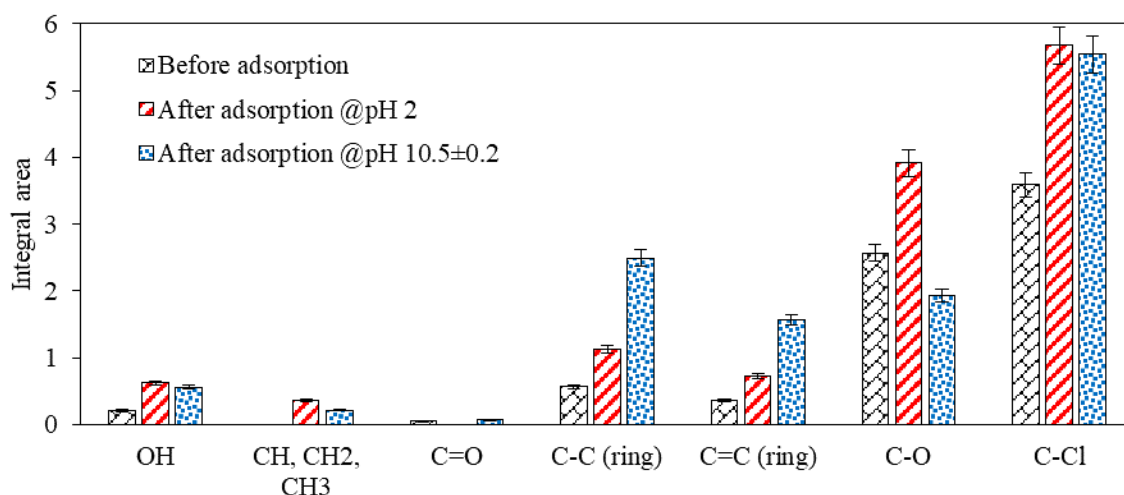
Figure 8. Integral area comparison of MAC before and after adsorption. Varied superscripts on bars denote statistical differences between extraction methods ($p < 0.05$)

3.4. Adsorption Kinetics and Thermodynamics

Thermodynamic parameters including the ΔH^o and ΔS^o values were calculated and presented in Table 3. Positive values of ΔH^o (9.68 kJ/mol) within the physisorption range of 0-20 kJ/mol suggested the presence of van der Waals forces between TCS and MAC, while positive values of ΔS^o (0.04 kJ/mol/K) confirmed an increase in the randomness of TCS molecules on the MAC surface. Negative values of ΔG^o for all five temperatures indicated that the adsorption reaction occurred spontaneously [27], confirming the TCS adsorption on MAC as an endothermic process.

Table 3. Thermodynamic parameters for adsorption of TCS onto MAC at different temperatures

Temperature (K)	In (K)	ΔH^o (kJ/mol)	ΔS^o (kJ/mol-K)	ΔG^o (kJ/mol)
298	1.19	9.68	0.04	-2.90
303	1.23	9.68	0.04	-3.11
308	1.27	9.68	0.04	-3.33
313	1.34	9.68	0.04	-3.54
318	1.45	9.68	0.04	-3.75

The resulting kinetic parameters are summarized in Table 4. Notably, the pseudo-second-order model exhibited a superior correlation ($R^2=0.9569$) compared to the pseudo-first-order model, suggesting that the adsorption of TCS onto MAC was primarily driven by electrostatic or van der Waals forces, and consistent with findings from the thermodynamics study.

Table 4. Kinetic parameters of TCS adsorption on MAC

$q_{e,exp}$ (mg/g)	Pseudo-first-order			Pseudo-second-order		
	q_e (mg/g)	k_1 (min^{-1})	R^2	q_e (mg/g)	k_2 (g/mg-min)	R^2
47.48	137.62	0.0075	0.9122	61.73	0.0001	0.9569

3.5. Fixed-bed Column Adsorption Experiments

3.5.1. Influence of Operating Conditions on Fixed-bed Column Adsorption

The fixed-bed column experiments encompassed variations in flow rate, initial concentration, and bed height, as outlined in Table 5. An increase in flow rate (6, 8, and 10 mL/min) and initial TCS concentration (20, 40, and 60 mg/L) resulted in a decrease in breakthrough time from 180 to 60 minutes. This occurred because a higher initial TCS concentration increased the concentration gradient of TCS between the adsorbent and bulk solution, leading to a stronger driving force. This decreased the mass transfer resistance between TCS and MAC, resulting in a shorter required saturation time [26]. The relationship between C_t/C_0 and time is depicted in Figures 9-a and 9-b, revealing an elevated adsorption capacity with an augmented flow rate and high initial TCS concentration. A flow rate of 10 mL/min and an initial TCS concentration of 60 mg/L demonstrated a maximum adsorption capacity of 34.94 mg/g at saturation time, with the breakthrough curve displaying a steeper initial segment and a slower adsorption rate towards the end due to

MAC saturation. This efficiency was attributed to the ability of the column to facilitate rapid mass transfer flux of the TCS bulk solution to the MAC surface, resulting in higher adsorption capacity due to an increased driving force and diffusion coefficient [13].

Results in Table 5 show a significant increase in bed height from 6 cm to 10 cm, resulting in an increase in breakthrough time (t_b) from 40 to 60 minutes, accompanied by an increase in saturation time (t_s) from 1,020 to 1,950 minutes and an increase in adsorption capacity from 21.29 to 34.94 mg/g, respectively. As shown in Figure 9-c, the breakthrough curves shifted from left to right, and the slope of the breakthrough curve became gentler, indicating that breakthrough time and saturation time increased. This was attributed to the increase in bed depth corresponding to a greater amount of adsorbent and providing more adsorption binding sites for TCS removal, thereby resulting in longer breakthrough and saturation times [26]. The non-sharp breakthrough curve, indicative of increased adsorption capacity, suggests prolonged residence times for TCS diffusion on the MAC surface.

Table 5. Parameters of the breakthrough curve in the fixed-bed column for TCS adsorption on MAC

Fixed-bed column condition			Parameters of breakthrough curve				
Q (ml/min)	C_0 (mg/L)	H (cm)	t_b (min)	t_s (min)	V_{eff} (L)	q_b (mg/g)	q_s (mg/g)
6	20	10	180	4,590	27.54	1.51	21.60
8	20	10	150	3,990	31.92	1.66	23.36
10	20	10	120	3,510	35.10	1.65	23.60
10	40	10	90	2,910	29.10	2.50	33.34
10	60	10	60	1,950	19.50	2.43	34.94
10	60	8	50	1,560	15.60	2.10	27.60
10	60	6	40	1,020	10.20	1.67	21.29

Consequently, a fixed-bed with a flow rate of 10 mL/min, an initial TCS concentration of 60 mg/L, and a bed height of 10 cm was selected for further experiments in pulsed-bed column adsorption, showcasing the highest adsorption capacity of 34.94 mg/g.

3.5.2. Analysis of Breakthrough Curves Using the Thomas and Yoon-Nelson Models

As illustrated in Figures 9-a to 9-c, the predicted parameters of the Thomas and Yoon-Nelson models were examined to align with the breakthrough curve under the various operational conditions shown in Table 6. The analysis revealed that the Thomas model coefficients exhibited high values ($R^2 = 0.9545$-0.9827) and proved adept at replicating the initial behavior of the breakthrough curve, demonstrating superior agreement with a higher R^2 compared to the Yoon-Nelson model. The Thomas model operates on the assumption that column adsorption adheres to the Langmuir isotherm and pseudo-second-order kinetics of batch adsorption, with no axial dispersion [34].

As the bed height increased, the k_{TH} value decreased from 0.092 to 0.043 mL/mg/min, while the q_{TH} increased from 36.15 to 40.35 mg/g for the Thomas model. Conversely, this led to a decrease in k_{YN} from 0.0056 to 0.0025 min^{-1} and an increase in τ from 501.39 to 948.68 minutes for the Yoon-Nelson model. These changes extended the column retention time and resulted in slower saturation of adsorption, attributed to the increase in bed depth, which induced higher axial dispersion and mass transport resistance [35, 36].

Table 6. Predicted model parameters for triclosan adsorption on MAC

| Fixed-bed condition			Thomas model			Yoon-Nelson model		
Q (mL/min)	C_0 (mg/L)	H (cm)	k_{TH} (mL/mg/min)	q_{TH} (mg/g)	R^2	k_{YN} (min^{-1})	τ (min)	R^2
6	20	10	0.065	21.70	0.9784	0.0013	2527.23	0.5806
8	20	10	0.069	22.95	0.9777	0.0014	1995.36	0.5978
10	20	10	0.076	23.32	0.9827	0.0015	1648.67	0.6538
10	40	10	0.052	36.51	0.9545	0.0020	1277.19	0.6036
10	60	10	0.043	40.35	0.9627	0.0025	948.68	0.5822
10	60	8	0.056	39.76	0.9602	0.0034	746.24	0.5822
10	60	6	0.092	36.15	0.9813	0.0056	501.39	0.6710
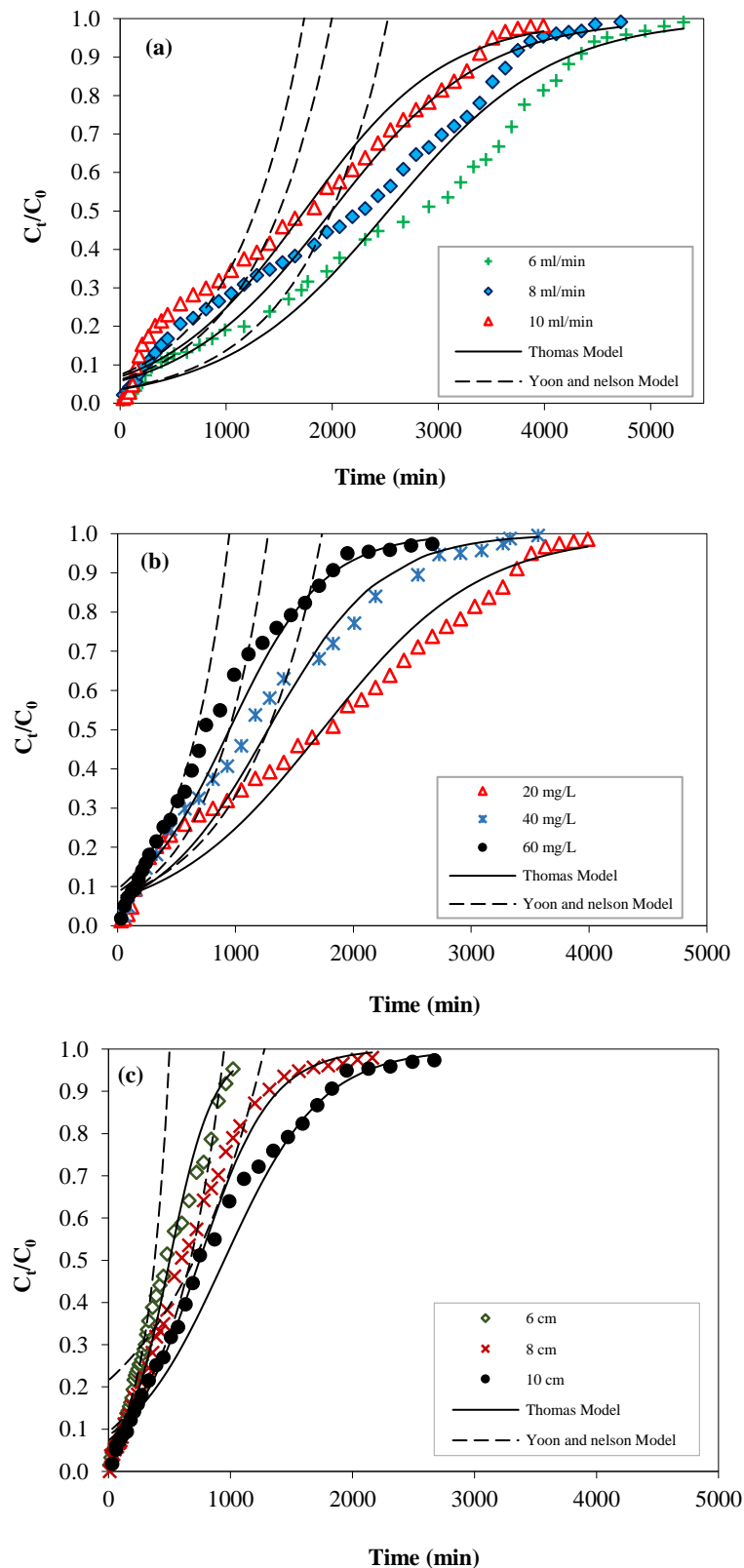
Figure 9. Breakthrough curves for TCS adsorption under varied (a) flow rates, (b) initial concentration, and (c) bed height
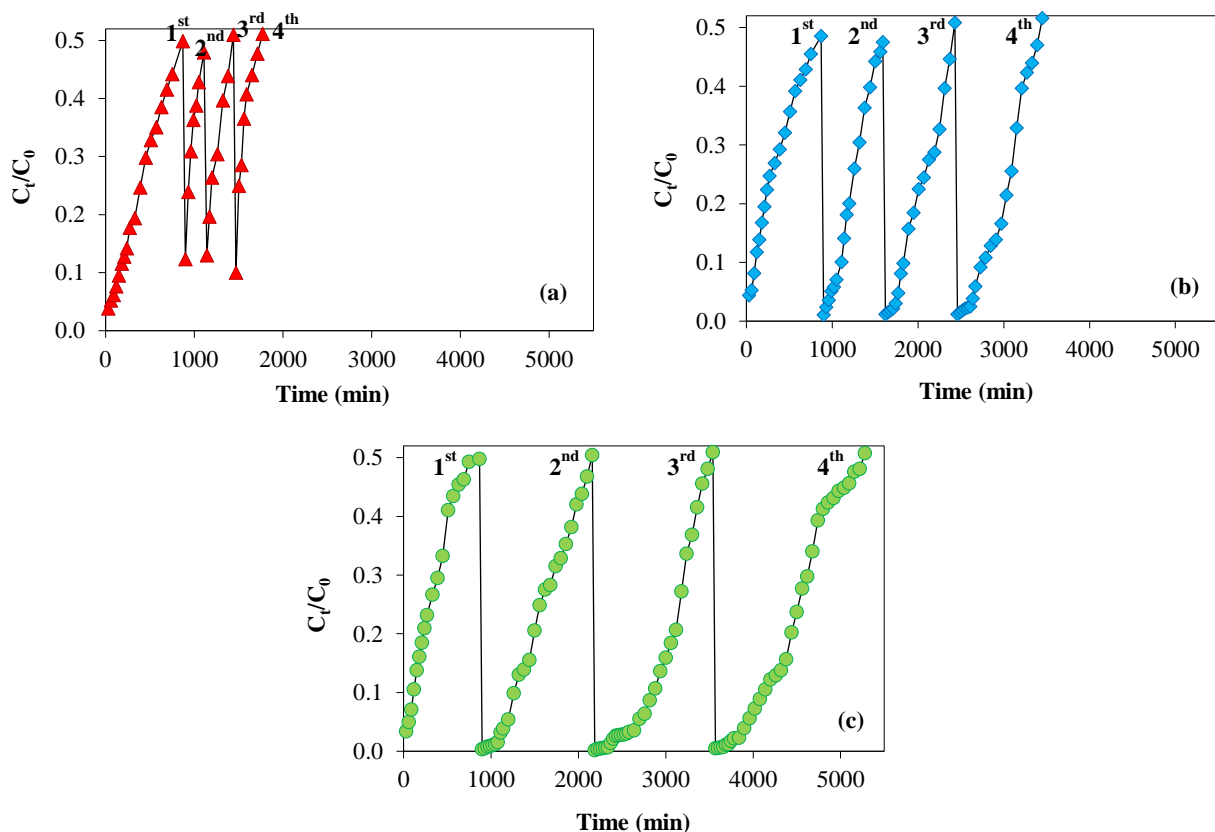
3.6. Pulsed-Bed Column Adsorption Experiments

3.6.1. Enhanced Adsorption Capacity and Extended Lifespan in Pulsed-Bed Columns

Breakthrough curve parameters in the pulsed-bed column experiments were calculated and summarized in Table 7. Findings indicated that an increase in the removed bed height at 2, 4, and 6 cm led to a rise in adsorption capacity ($q_{0.5}$) to 31.99, 50.76, and 62.60 mg/g, respectively. As shown in Figures 10-a to 10-c, an increase in the removed pulsed-bed height was reflected in the breakthrough curves extending from left to right on the time scale, respectively. The slope of

Civil Engineering Journal

Vol. 10, No. 05, May, 2024

the breakthrough curve became gentler, indicating an increase in breakthrough time and saturation time [36]. Therefore, this significantly contributed to extending the lifespan of the column from 1,770 to 5,280 minutes, compared to the lifespan of the fixed-bed column at 870 minutes.

Table 7. Breakthrough curve parameters in the pulsed-bed column for TCS adsorption on MAC

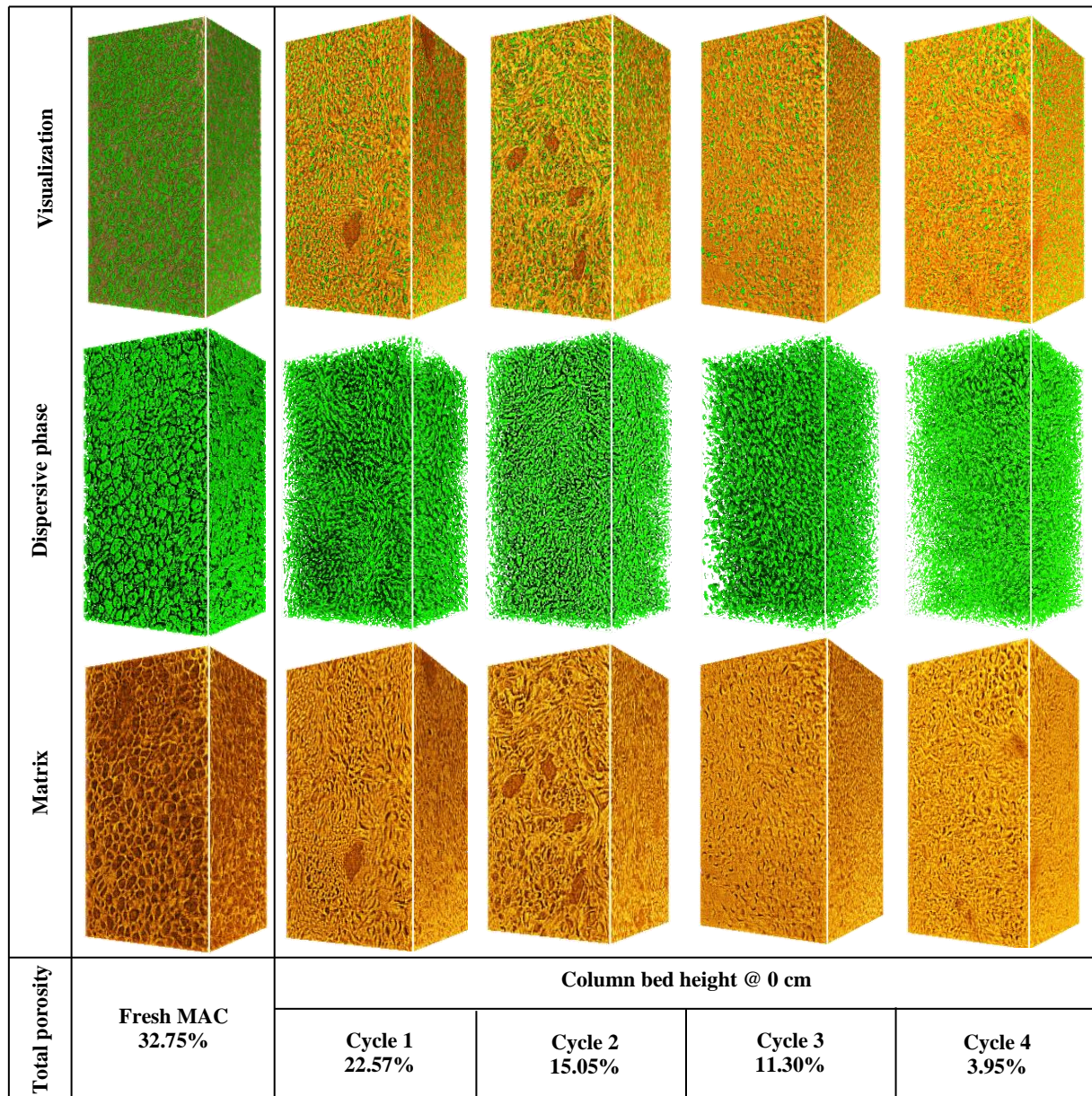| Pulsed-bed height (cm)	Cycle	t_b (min)	$t_{0.5}$ (min)	V_{eff} (L)	q_b (mg/g)	$q_{0.5}$ (mg/g)
0	1	60	870	8.7	2.43	25.63
2	1	60	870	8.7	2.45	26.72
	2	-	1,110	11.1	-	27.83
	3	-	1,440	14.4	-	30.41
	4	-	1,770	17.7	-	31.99
4	1	60	870	8.7	2.47	25.87
	2	990	1,560	15.6	22.07	34.76
	3	1,770	2,430	24.3	31.64	42.97
	4	2,670	3,450	34.5	39.76	50.76
6	1	60	870	8.7	2.50	25.30
	2	1,200	2,160	21.6	24.50	42.80
	3	2,700	3,540	35.4	41.50	53.50
	4	4,320	5,280	52.8	53.40	62.60

Figure 10. Breakthrough curves for TCS adsorption in a pulsed-bed column at various removed-bed heights (a) 2 cm, (b) 4 cm, and (c) 6 cm

3.6.2. Clogging Pattern Analysis of Pulsed-Bed Column

Figure 11 presents a 3D visualization derived from XTM analysis of contaminated MAC in the pulsed-bed column. Changes were made by removing the used MAC and replacing it with fresh MAC in every cycle. The total porosity by volume of fresh MAC and contaminated MAC in cycles 1, 2, 3, and 4 was measured, showing a decreasing trend as 32.75%, 22.57%, 15.05%, 11.30%, and 3.95%, respectively. These findings suggested that, at the upper bed height of each cycle, sufficient active sites for TCS adsorption were still maintained.

The XTM analysis evaluated the ratio of open and closed pores, where 'open pores' represent the adsorbable active sites on MAC, and 'closed pores' refer to pores that are not connected with others or are non-active sites, posing a potential problem for decreasing active sites and adsorption capacity because the adsorbate molecules cannot transfer within this area. The results indicated a potential issue for decreasing active sites and adsorption capacity.

Total porosity	Fresh MAC 32.75%	Column bed height @ 0 cm			
		Cycle 1 22.57%	Cycle 2 15.05%	Cycle 3 11.30%	Cycle 4 3.95%

Figure 11. 3D visualization of fresh and contaminated MAC in each cycle using XTM analysis in the pulsed-bed column

Results revealed that fresh MAC had a total pore volume of 32.75%, consisting of a closed pore volume of 8.27% and an open pore volume of 24.48%. As depicted in Figure 12, after the 4th cycle of operation, the open pore volume of contaminated MAC exhibited an increasing trend of 13.92%, 10.62%, 2.52%, and 0.51%, with varied bed depths of 0, 3, 6, and 9 cm, respectively. The remaining total pore volume of the contaminated MAC increased proportionally with column bed height: 3.95%, 7.14%, 9.95%, and 11.29%, respectively. These findings indicated that the open pores of the pulsed-bed column were almost filled, while the closed pores remained, causing clogging.

The observed trend suggested that clogging initiates from the bottom and progresses upwards in the column. This phenomenon was attributed to up-flow feeding, causing the MAC at the bottom to saturate and accumulate more rapidly than in the upper part of the column. Results revealed that MAC columns at bed depths of 6 and 9 cm exhibited sufficient total pore volumes of 9.95% and 11.29%, respectively. These findings suggested that the MAC column at greater depths can retain more pollutants and resist clogging. The efficacy of the pulsed-bed column,

when removing only the 6 cm bottom portion of the column instead of the entire column, was highlighted. This approach extended the lifespan of the column from 1,950 minutes for the fixed-bed to 5,280 minutes for the pulsed-bed and increased the adsorption capacity from 33.34 mg/g for the pulsed-bed to 53.40 mg/g for the fixed-bed. These results suggested practical applications, especially in industrial-scale settings utilizing pulsed-bed columns. The findings can be instrumental in optimizing performance, minimizing adsorbent consumption, and maximizing longevity.
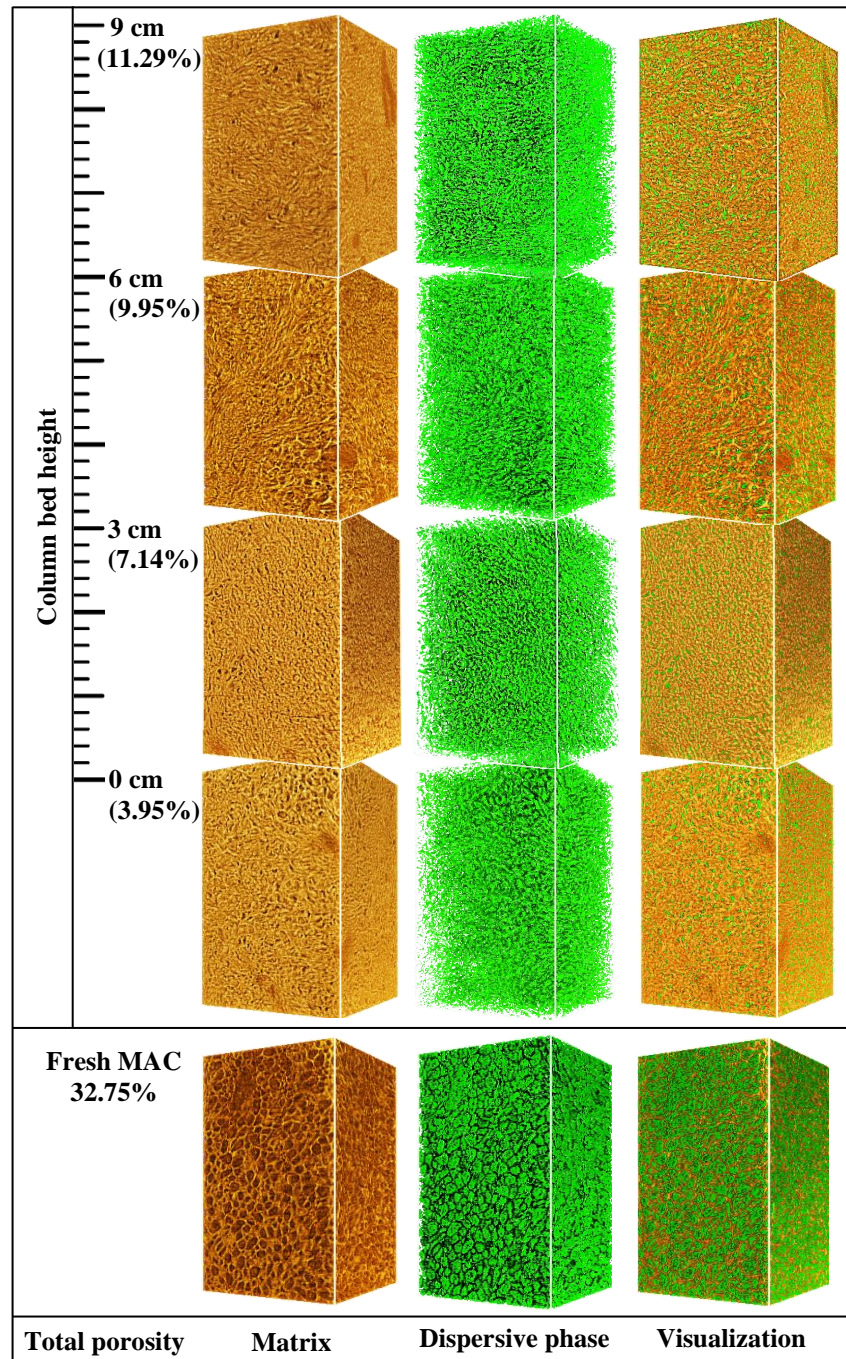

Figure 12. XTM analysis of fresh and contaminated MAC columns at bed depths of 0, 3, 6, and 9 cm

4. Conclusion

Macadamia nut shell activated carbon (MAC) demonstrated significant potential as a cost-effective adsorbent, highlighting the utilization of agricultural waste. MAC effectively adsorbed TCS with a high capacity of 119.05 mg/g under optimal conditions of contact time of 780 minutes, initial TCS concentration of 20 mg/L, agitation speed of 150 rpm, pH 2, and 45°C. The kinetics of adsorption followed a pseudo-second-order model, and the equilibrium data fitted well with both the Langmuir and Freundlich isotherm models.

In fixed-bed column operation under the specific conditions of flow rate 10 mL/min, initial TCS concentration 60 mg/L, and bed column height 10 cm, the highest adsorption capacity was 34.94 mg/g, with an exhaustion time of 1,950 minutes. The superior performance of the pulsed-bed column with a removed bed height of 6 cm led to a rise in adsorption capacity of 53.40 mg/g, coupled with an extended operational lifespan of 5,280 minutes. These findings rendered the pulsed-bed column suitable for TCS removal from wastewater in the personal care product industry. In terms of industrial applications, the pulsed-bed column was proven successful in extending the operational lifespan of the column, increasing the adsorption capacity, and minimizing adsorbent consumption.

5. Declarations

5.1. Author Contributions

Conceptualization, J.Y.; methodology, J.Y. and S.N.; software, S.N. and M.P.; validation, J.Y. and S.N.; formal analysis, M.P. and S.N.; investigation, J.Y. and M.P.; resources, J.Y.; data curation, J.Y. and M.P.; writing—original draft preparation, M.P.; writing—review and editing, J.Y.; visualization, M.P. and S.N.; supervision, J.Y.; project administration, J.Y.; funding acquisition, J.Y. All authors have read and agreed to the published version of the manuscript.

5.2. Data Availability Statement

Data presented in this study are available on reasonable request from the corresponding author.

5.3. Funding

5.4. Acknowledgements

5.5. Conflicts of Interest

The authors declare no conflict of interest.

6. References

[1] Mhlongo, S. A., Sibali, L. L., & Ndibewu, P. P. (2023). Occurrence, quantification and removal of triclosan in wastewater of Umbogintwini Industrial Complex in KwaMakhutha, South Africa. South African Journal of Science, 119(11–12), 1-9. doi:10.17159/sajs.2023/14743.

[2] Zhang, Q., Kroeze, C., Cui, S., Li, Y., Ma, L., Strokal, V., Vriend, P., Wang, M., van Wijnen, J., Xu, W., Zhang, F., & Strokal, M. (2024). COVID-19 estimated to have increased plastics, diclofenac, and triclosan pollution in more than half of urban rivers worldwide. Cell Reports Sustainability, 1(2023), 100001. doi:10.1016/j.crsus.2023.100001.

[3] Milanović, M., Đurić, L., Milošević, N., & Milić, N. (2023). Comprehensive insight into triclosan—from widespread occurrence to health outcomes. Environmental Science and Pollution Research, 30(10), 25119–25140. doi:10.1007/s11356-021-17273-0.

[4] Dar, O. I., Aslam, R., Pan, D., Sharma, S., Andotra, M., Kaur, A., Jia, A. Q., & Faggio, C. (2022). Source, bioaccumulation, degradability and toxicity of triclosan in aquatic environments: A review. Environmental Technology & Innovation, 25. doi:10.1016/j.eti.2021.102122.

[5] Sinicropi, M. S., Iacopetta, D., Ceramella, J., Catalano, A., Mariconda, A., Pellegrino, M., Saturnino, C., Longo, P., & Aquaro, S. (2022). Triclosan: A Small Molecule with Controversial Roles. Antibiotics, 11(6), 735. doi:10.3390/antibiotics11060735.

[6] Jabłońska-Trypuć, A. (2023). A review on triclosan in wastewater: Mechanism of action, resistance phenomenon, environmental risks, and sustainable removal techniques. Water Environment Research, 95(9). doi:10.1002/wer.10920.

[7] Lee, J. S., Lee, J. S., & Kim, H. S. (2024). Toxic effects of triclosan in aquatic organisms: A review focusing on single and combined exposure of environmental conditions and pollutants. Science of the Total Environment, 920. doi:10.1016/j.scitotenv.2024.170902.

[8] Li, L. (2021). Toxicity evaluation and by-products identification of triclosan ozonation and chlorination. Chemosphere, 263. doi:10.1016/j.chemosphere.2020.128223.

[9] Phuekphong, A. F., Imwiset, K. J., & Ogawa, M. (2020). Organically Modified Bentonite as an Efficient and Reusable Adsorbent for Triclosan Removal from Water. Langmuir, 36(31), 9025–9034. doi:10.1021/acs.langmuir.0c00407.

[10] Medellin-Castillo, N. A., González-Fernández, L. A., Ocampo-Pérez, R., Leyva-Ramos, R., Luiz-Dotto, G., Ramírez, R. F., Navarro-Frómeta, A. E., Aguilera-Flores, M. M., Carrasco-Marín, F., Hernández-Mendoza, H., & Aguirre-Contreras, S. (2022). Removal of triclosan from water by adsorption on activated carbons and photodegradation. Research Square (Preprint), 1-46. doi:10.21203/rs.3.rs-1440179/v1.

[11] Duque-Brito, E., Lobato-Peralta, D. R., Okolie, J. A., Arias, D. M., Sebastian, P. J., & Okoye, P. U. (2024). Fast-kinetics adsorption of a binary solution containing cationic and ionic pollutants using high-surface area activated carbon derived from macadamia nutshell. Energy, Ecology and Environment, 9(1), 84–99. doi:10.1007/s40974-023-00304-6.

[12] Wongcharee, S., Aravinthan, V., Erdei, L., & Sanongraj, W. (2018). Mesoporous activated carbon prepared from macadamia nut shell waste by carbon dioxide activation: Comparative characterisation and study of methylene blue removal from aqueous solution. Asia-Pacific Journal of Chemical Engineering, 13(2). doi:10.1002/apj.2179.

[13] Machedi, S., Ejidike, I. P., Mtunzi, F. M., Pakade, V. E., & Klink, M. J. (2019). Chlorinated Phenols Sorption Performance by Macadamia Activated Carbon and Grafted Macadamia Activated Carbon: Characterization, Kinetics, and Thermodynamic studies. Oriental Journal of Chemistry, 35(5), 1469–1479. doi:10.13005/ojc/350501.

[14] Al Mesfer, M. K., Danish, M., Khan, M. I., Ali, I. H., Hasan, M., & Jery, A. El. (2020). Continuous fixed bed co2 adsorption: Breakthrough, column efficiency, mass transfer zone. Processes, 8(10), 1233. doi:10.3390/pr8101233.

[15] AL-Doury, M. M. I., & Alwan, M. H. (2021). Phenol Removal from Synthetic Wastewater by Adsorption Column. IOP Conference Series: Materials Science and Engineering, 1058(1), 012034. doi:10.1088/1757-899x/1058/1/012034.

[16] Sazali, N., Harun, Z., & Sazali, N. (2020). A review on batch and column adsorption of various adsorbent towards the removal of heavy metal. Journal of Advanced Research in Fluid Mechanics and Thermal Sciences, 67(2), 66–88.

[17] Patel, H. (2019). Fixed-bed column adsorption study: a comprehensive review. Applied Water Science, 9(3), 45. doi:10.1007/s13201-019-0927-7.

[18] Plangklang, C., & Sookkumnerd, T. (2023). Modelling and feedforward control of pulsed bed adsorption column for colorant removal in sugar syrup. Engineering Journal, 27(1), 29–38. doi:10.4186/ej.2023.27.1.29.

[19] Wyllie, G. R. A. (2015). Spectroscopic determination of triclosan concentration in a series of antibacterial soaps: A first-year undergraduate laboratory experiment. Journal of Chemical Education, 92(1), 153–156. doi:10.1021/ed5004146.

[20] Kaur, I., Gaba, S., Kaur, S., Kumar, R., & Chawla, J. (2018). Spectrophotometric determination of triclosan based on diazotization reaction: Response surface optimization using box-behnken design. Water Science & Technology, 77(9), 2204–2212. doi:10.2166/wst.2018.123.

[21] Khader, E. H., Khudhur, R. H., Abbood, N. S., & Albayati, T. M. (2023). Decolourisation of Anionic Azo Dye in Industrial Wastewater Using Adsorption Process: Investigating Operating Parameters. Environmental Processes, 10(2), 34. doi:10.1007/s40710-023-00646-7.

[22] Karthika, M., & Vasuki, M. (2021). Comparative Study of Adsorption of Different Dyes from Aqueous Media onto Physically Activated Carbon: Isotherm, Kinetic and Thermodynamic Parameter. International Journal of Applied Engineering, 16(6), 441–446.

[23] Ndagijimana, P., Liu, X., Li, Z., Yu, G., & Wang, Y. (2020). The synthesis strategy to enhance the performance and cyclic utilization of granulated activated carbon-based sorbent for bisphenol A and triclosan removal. Environmental Science and Pollution Research, 27(13), 15758–15771. doi:10.1007/s11356-020-08095-7.

[24] Sun, K., Li, S., Waigi, M. G., & Huang, Q. (2018). Nano-MnO2-mediated transformation of triclosan with humic molecules present: kinetics, products, and pathways. Environmental Science and Pollution Research, 25(15), 14416–14425. doi:10.1007/s11356-018-1637-7.

[25] Sultana, M., Rownok, M. H., Sabrin, M., Rahaman, M. H., & Alam, S. M. N. (2022). A review on experimental chemically modified activated carbon to enhance dye and heavy metals adsorption. Cleaner Engineering and Technology, 6. doi:10.1016/j.clet.2021.100382.

[26] Vidovix, T. B., Januário, E. F. D., Araújo, M. F., Bergamasco, R., & Vieira, A. M. S. (2022). Investigation of two new low-cost adsorbents functionalized with magnetic nanoparticles for the efficient removal of triclosan and a synthetic mixture. Environmental Science and Pollution Research, 29(31), 46813–46829. doi:10.1007/s11356-022-19187-x.

[27] Triwiswara, M., Lee, C. G., Moon, J. K., & Park, S. J. (2020). Adsorption of triclosan from aqueous solution onto char derived from palm kernel shell. Desalination and Water Treatment, 177, 71–79. doi:10.5004/dwt.2020.24872.

[28] Rodrigues, L. A., De Sousa Ribeiro, L. A., Thim, G. P., Ferreira, R. R., Alvarez-Mendez, M. O., & Coutinho, A. D. R. (2013). Activated carbon derived from macadamia nut shells: An effective adsorbent for phenol removal. Journal of Porous Materials, 20(4), 619–627. doi:10.1007/s10934-012-9635-5.

[29] Dan, S., & Chattree, A. (2021). Influence of modifiers on point of zero charge (pHPZC) of PMMA modified and PMMA-PEG modified MnFe2O4 nanoparticles. International Journal of New Innovations in Engineering and Technology. 17(2), 25-29.

[30] Alvarez-Garciá, S., MacEdo-Miranda, G., Martínez-Gallegos, S., Ordoñez-Regíl, E., López-Castillo, J., & Aguirre-Miranda, E. (2020). Removal of triclosan by CTAB-modified zeolite-rich tuff from aqueous solutions. MRS Advances, 5, 3257–3264. doi:10.1557/adv.2020.394.

[31] Li, Q., Huang, L., Zhu, P., Zhong, M., & Xu, S. (2023). Rapid adsorption of triclosan and p-chloro-m-xylenol by nitrogen-doped magnetic porous carbon. Environmental Science and Pollution Research, 30(1), 1640–1655. doi:10.1007/s11356-022-22084-y.

[32] Kaur, H., Bansiwal, A., Hippargi, G., & Pophali, G. R. (2018). Effect of hydrophobicity of pharmaceuticals and personal care products for adsorption on activated carbon: Adsorption isotherms, kinetics and mechanism. Environmental Science and Pollution Research, 25(21), 20473–20485. doi:10.1007/s11356-017-0054-7.

[33] Almeida-Naranjo, C. E., Cuestas, J., Guerrero, V. H., & Villamar-Ayala, C. A. (2024). Efficient Decontamination: Caffeine/Triclosan Removal using Rice Husk in Batch and Fixed-Bed Columns. Water (Switzerland), 16(2), 197. doi:10.3390/w16020197.

[34] Patel, H. (2020). Batch and continuous fixed bed adsorption of heavy metals removal using activated charcoal from neem (Azadirachta Indica) leaf powder. Scientific Reports, 10(1), 16895. doi:10.1038/s41598-020-72583-6.

[35] Thrikkykkal, H., Antu, R., & Harikumar, P. S. (2023). Remediation of Pb (II), Cd (II), and Zn (II) from aqueous solutions using porous (styrene–divinylbenzene)/Cu–Ni bimetallic nanocomposite microspheres: continuous fixed-bed column study. Water Science and Technology, 87(9), 2277–2291. doi:10.2166/wst.2023.101.

[36] Li, Y., Gong, F., Yang, W., & Liu, B. (2023). Effective triclosan removal by using porous aromatic frameworks in continuous fixed-bed column studies. Environmental Science and Pollution Research, 30(57), 121007–121013. doi:10.1007/s11356-023-30714-2.